



Sorption Behavior of Zirconium Ions from Aqueous Solutions Using Different Inorganic Sorbents Based on Titanate

M. R. Abass¹ · A. B. Ibrahim¹ · M. M. Abou-Mesalam¹

Received: 4 September 2023 / Accepted: 22 April 2024
© The Author(s) 2024

Abstract

In this article, we explore the sorption behavior of Zr(IV) ions by lithium titanate (LiTi), magnesium titanate (MgTi), and lithium magnesium titanate (LiMgTi) sorbents. These sorbents, fabricated using the precipitation method, were used for the Zr(IV) sorption from aqueous solutions. We employed various analytical tools, including XRD, FT-IR, BET, SEM, and EDX, to examine the prepared sorbents' structure, morphology, and functional groups. We also studied the effect of pH, time, initial metal concentrations, temperature, and interfering species on sorption. The kinetic data obey pseudo-first-order. Many isotherm models were utilised to investigate equilibrium data. The results of thermodynamic functions show an endothermic and spontaneous sorption process. Finally, the influence of the interfering species reveals that as the concentration of CaCl₂, MgCl₂, and NaCl increases, the Zr(IV) adsorption rate decreases. The investigation demonstrated that LiMgTi is suitable for retaining Zr(IV) from aqueous solutions and could purify effluent polluted with Zr(IV) ions.

Keywords Zr(IV) · LiTi · MgTi · LiMgTi · Kinetic · Thermodynamic

1 Introduction

Contaminant uptake from wastewater has recently emerged as one of the most pressing issues, as its relevance grows with increased industrial activity [1, 2]. Many types of radioactive waste can be generated while operating nuclear reactors and radiological facilities. Nuclear fission generates isotopes such as ¹³⁷Cs, ⁹⁰Sr, ⁹⁵Zr, ¹⁴⁴Ce, ¹⁵²⁺¹⁵⁴Eu, or ¹⁰⁶Ru, which can accumulate in the geospheres and biospheres in the event of a nuclear catastrophe, nuclear weapons test sites, and waste storage facilities [3–5]. Because of their negative impact, wastewater must be treated before being discharged into the environment [6]. The commonly used technologies include chemical precipitation [7, 8], physical treatment like solvent extraction [9], adsorption [10], biosorption [11], membrane [12], and ion exchange [13]. Sorption is regarded as the most promising technique for radioactive wastewater treatment. It can reduce large volumes of waste into a more

stable solid form considering its ease of use, affordability, effectiveness, and high capacity [14].

Plutonium uranium redox extraction (PUREX) is the only commercial technique used worldwide in nuclear fuel reprocessing plants. It is primarily based on the substantial disparity in the extraction capacity of the extractant tributyl phosphate (TBP) for uranium, thorium, neptunium, plutonium, and their fission products in various oxidation states, thus enabling the purification and separation of these elements. The solution resulting from the dissolution of spent nuclear fuel will contain a notable Zr(IV) concentration, given its frequent use as the cladding material for fuel rods. Simultaneously, due to fission reactions, elements like uranium and plutonium in spent fuel undergo nuclear fission, producing a range of fission products, including isotopes of Zr(IV). Within the PUREX process, Zr(IV) can undergo a reaction with the radiolysis products of TBP and alkane diluents, resulting in the formation of a viscous emulsion [15] at the interface of the organic and aqueous phases, commonly known as “crud” [16]. The formation of crud reduces the recovery and purity of uranium and plutonium and hastens the decomposition of the extractant, thereby hindering the normal production process [17]. Studies on the % uptake of Zr(IV) ions from aqueous solutions have been focused largely on ion exchange and surface adsorption

✉ M. R. Abass
mohamed.ragab2014300@yahoo.com

¹ Egyptian Atomic Energy Authority, Hot Laboratories and Waste Management Centre, Cairo 13759, Egypt

Table 1 Conditions for the synthesis of LiTi, MgTi, and LiMgTi sorbents

Sorbents	LiCl	MgCl ₂ ·6H ₂ O	TiCl ₄
LiTi	150	0	150
MgTi	0	150	150
LiMgTi	150	75	75

[18]. Many adsorbent materials were used for the adsorption of Zr(IV) include thermally activated natural bentonite (TANB) adsorbent with adsorption capacity of 15.432 mg/g [19], hyper cross linkage phosphothiol polymer (HCPTP) adsorbent with a maximum adsorption capacity of 307 mg/g [20], and hydrated manganese oxide (HMO) adsorbent with adsorption capacity of 665.7 mg/g [21].

Inorganic sorbents outperform traditional radioactive waste treatment applications, exhibiting high affinity and enhanced radiation, chemical, and thermal stability [22]. Some effective approaches for radionuclide sequestration applications include synthetic zeolites [23], sodium titanates [24], metal oxides [25], silicotitanates [26], transition metal hexacyanoferrates [27, 28], and metal-organic framework-based adsorbents [29, 30]. Previously, sodium titanates [24] and silicotitanates composites [18] were prepared earlier, but LiTi, MgTi, and LiMgTi sorbent materials were not prepared.

In this work, LiTi, MgTi, and LiMgTi sorbents were prepared as novel materials and used for the adsorption of Zr(VI) ions from aqueous solutions. Different analytical analyses were used to characterise the LiTi, MgTi, and LiMgTi sorbents. Many parameters, including the effect of pH, time, initial metal concentrations, temperature, and interfering species on sorption, were studied to attain the optimum conditions for Zr(VI) ions sorption.

2 Experimental

2.1 Materials

LiCl (PioChem, Egypt), MgCl₂·6H₂O and TiCl₄ (Loba Chemie, India), ZrOCl₂ (Alpha Chemika, India), HCl, and

HNO₃ (Merck, Germany). All solvents, double-distilled water (DDW), and reagents utilised in this work were analytical grades and were used without additional cleaning.

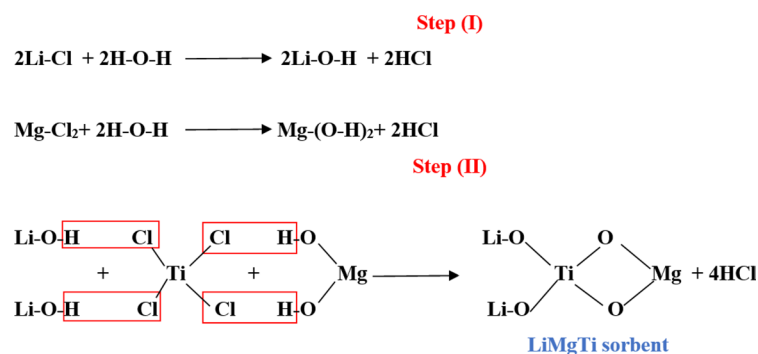
2.2 Preparation

In this work, LiTi, MgTi, and LiMgTi were fabricated by dropwise addition of 0.5 M LiCl solution and 0.5 M MgCl₂·6H₂O solutions to 10% V/V TiCl₄ (soluble in 4 M HCl) in diverse volumetric ratios, as represented in Table 1. After adding the elements with fixed stirring for 120 min, NH₃ solution (10%) was added to the mixture, and colour gels were generated at pH ranges (7-7.5). The mixtures were left undisturbed overnight, rinsed with DDW, and dried at 60 ± 1 °C. The formation mechanism of the LiMgTi sorbent is carried out through two steps, as represented in Scheme 1.

- (I) A reaction was carried out between LiCl and MgCl₂·6H₂O with H₂O to form LiOH and Mg(OH)₂ by eliminating HCl.
- (II) LiMgTi sorbent was formed by a reaction between 2LiOH and Mg(OH)₂ and TiCl₄ solution, with the elimination of four molecules of HCl (4 chloride ions linked with titanium and 4 hydrogen ions linked with 2LiOH and Mg(OH)₂). These data are confirmed by ATR analysis, as seen later.

2.3 Instruments for Sorbent Characterisation

A Bruker XRD diffractometer D2 Phaser II, Germany, was used to measure the x-ray diffraction patterns of LiTi, MgTi, and LiMgTi sorbents. A computerised spectrophotometer in the range of 4000–400 cm⁻¹ (Fourier transformed infrared (FTIR) spectrum, Alpha II Bruker, Germany) was used to determine bonds between atoms and function groups in LiTi, MgTi, and LiMgTi sorbents. The sorbent's specific surface area and pore size distribution were determined using N₂ adsorption/desorption isotherm at 77 K by Quantachrome Nova instrument, Model 184 Nova1000e series, USA. The amount of N₂ adsorbed onto the LiTi, MgTi, and

Scheme 1 Formation mechanism of LiMgTi sorbent

LiMgTi sorbents was used to calculate the specific surface area (S_{BET}) utilising the BET equation. The morphologies and the elemental analysis of the LiTi, MgTi, and LiMgTi sorbents were investigated using a scanning electron microscope (SEM) and energy-dispersive X-ray (EDX) analysis model (ZEISS - EVO 15, UK).

2.4 Instruments for Sorbate Analysis

The Zr(IV) concentrations were determined using a Shimadzu UV-Visible Recording Spectrophotometer (UV-160 A) produced and supplied by Shimadzu Kyoto, Japan.

2.5 Chemical Stability

0.2 g of solid and 20 mL of different solvents were shaken for around 3 days at 25 ± 1 °C to study the chemical stability of the LiTi, MgTi, and LiMgTi sorbents using diverse solvents such as mineral acids, alkaline, and some organic solvents. The gravimetric analysis determined the amount of LiTi, MgTi, and LiMgTi sorbents [13, 18, 31, 32].

2.6 Sorption Investigations

Many parameters such as pH (0.5–2.4), mixing time (5 min–3 h), initial metal concentrations (25–500 mg/L), and reaction temperatures (298–338 K) are checked to get the optimal condition for sorption. The LiTi, MgTi, and LiMgTi sorbents and Zr(IV) solution were contacted in a batch method by mixing 0.05 g of LiTi, MgTi, and LiMgTi sorbents with 5 mL of Zr(IV) of the start concentration of 50 mg/L in a shaker thermostat (Kottermann D-1362, Germany). The sorption efficiency (% S.E.) and the adsorption capacities at any time t (q_t), mg/g and equilibrium (q_e), mg/g retained on the LiTi, MgTi, and LiMgTi sorbents were detected utilising the following equations; respectively [33–35]:

$$\% \text{ S.E.} = \left(\frac{C_o - C_f}{C_o} \right) 100 \quad (1)$$

$$q_t = (C_o - C_t) \frac{V}{m} \quad (2)$$

$$q_e = (C_o - C_e) \frac{V}{m} \quad (3)$$

Where C_o , C_f , C_e , and C_t are the initial concentration, final concentration, equilibrium concentration, and concentration at any time t of the Zr(IV) (mg/L), respectively; V is the volume of the solution (L), and m is the mass of the dried adsorbent (g).

2.7 Saturation Capacity

Repeated batch equilibration of 100 mg/L Zr(IV) with LiTi, MgTi, and LiMgTi sorbents was performed until no further sorption of Zr(IV) for saturation capacity detection. The saturated capacity of the LiTi, MgTi, and LiMgTi sorbents equals the total summation of successive amounts sorbed (q_e), mg/g computed from Eq. (3). It could be determined by applying Eq. (4).

$$\text{Saturation capacity} = \sum_{e=1}^n q_e \quad (4)$$

Where n is the summation number of times new volumes were added.

2.8 The Distribution Coefficients

The distribution coefficients (K_d), mL/g as a function of pH were computed with the Eq. (5) [33, 36]:

$$K_d = \left(\frac{C_o - C_f}{C_f} \right) \frac{V}{m} \quad (5)$$

V is the solution volume (mL).

2.9 Kinetic Investigation

To describe the mechanism of the adsorption process, the nonlinear form of the pseudo-first-order (PFO) (Eq. (6)), pseudo-second-order (PSO) (Eq. (7)), and Elovich (Eq. (8)), rate model's equations were used in the experimental data. The PFO model is a solid-liquid system model derived from the adsorption capacity of the adsorbent [37]. The PSO model is based on the number of active centres on the adsorbent surface and the solid phase adsorption capacity [38]. The Elovich equation is often utilised for chemisorption, and it is most likely the mechanism that governs the adsorption rate [39].

$$q_t = q_e [1 - \exp(-K_1 t)] \quad (6)$$

$$q_t = \frac{q_e^2 K_2 t}{1 + q_e K_2 t} \quad (7)$$

$$q_t = \frac{1}{\beta} \ln(1 + \alpha \beta t) \quad (8)$$

q_t : the amount sorbed at time t (mg/g), q_e : the amount sorbed at equilibrium (mg/g), t : time (min), K_1 : the rate constant of the PFO (min^{-1}), K_2 : the rate constant of the PSO model ($\text{g mg}^{-1} \text{min}^{-1}$). α and β : Elovich constants represent the initial

sorption rate ($\text{g mg}^{-1} \text{min}^{-2}$) and desorption constant ($\text{mg g}^{-1} \text{min}^{-1}$). Initial rates for the PFO and PSO adsorption models were calculated from Eqs. (9) and (10), respectively.

$$H_1 = K_1 q_e \quad (9)$$

$$H_2 = K_2 q_e^2 \quad (10)$$

H_1 is the initial adsorption rate for PFO ($\text{mg g}^{-1} \text{min}^{-1}$), and H_2 is the initial adsorption rate for PSO ($\text{mg g}^{-1} \text{min}^{-1}$).

2.10 Isotherms Modelling

The concentration results obtained to determine the isotherms of the Zr(IV) loaded onto LiTi, MgTi, and LiMgTi sorbents were analysed using a nonlinear form of Langmuir (Eqs. (11 and 12)), Freundlich (Eq. (13)), and Langmuir–Freundlich isotherm models (Eq. (14)). In the presence of initial concentrations varying from (25–500 mg/L) at optimum pH 2.4, sorption isotherms were performed. The Langmuir isotherm model assumes that the active centres of adsorption are uniformly distributed across the adsorbent surface [40]. The Freundlich isotherm model explains hyperbolic adsorption behaviour and provides information about adsorbent surface heterogeneity [41]. Langmuir–Freundlich isotherm model is suitable for chemisorption adsorbate ions onto heterogeneous surfaces. It reduces to the Freundlich isotherm model at low adsorbate concentrations, while at high concentrations, it approaches the Langmuir isotherm model [42].

$$q_e = q_m \frac{K_L C_e}{1 + K_L C_e} \quad (11)$$

$$R_L = \frac{1}{1 + K_L C_o} \quad (12)$$

$$q_e = K_F C_e^{1/n} \quad (13)$$

$$q_e = \frac{q_m (K_{LF} C_e)^m}{1 + (K_{LF} C_e)^m} \quad (14)$$

q_m is the maximum adsorption capacity (mg/g), K_L is the parameter for the Langmuir isotherm, R_L is the separation factor, K_F is the Freundlich constant, $1/n$ is the adsorbent surface heterogeneity, K_{LF} is Langmuir–Freundlich isotherm constant (L mg^{-1}) and m is an empirical parameter that lies between 0 and 1. Langmuir–Freundlich isotherm model converts to Langmuir isotherm model when m values equal unity, while it becomes nearer to Freundlich isotherm model when m deviates from unity.

2.11 Influence of Temperature

Calculating thermodynamic parameters is useful to see whether the adsorption process is spontaneous. In addition to this, we can easily show the temperature effect on the Zr(IV) sorbed onto LiTi, MgTi, and LiMgTi sorbents thanks to thermodynamic parameters at different reaction temperatures (298, 308, 318, 328, and 338 K), the % sorption of Zr(IV) sorbed onto LiTi, MgTi, and LiMgTi sorbents was studied at pH 2.4 to calculate the thermodynamic parameters. For the calculation of enthalpy (ΔH°), entropy (ΔS°), and Gibbs free energy (ΔG°) parameters regarding the adsorption process, we used the following equations [43–45];

$$\Delta G^\circ = -RT \ln(K_d) \quad (15)$$

$$\ln K_d = \frac{\Delta S^\circ}{R} - \frac{\Delta H^\circ}{RT} \quad (16)$$

$$\Delta G^\circ = \Delta H^\circ - T\Delta S^\circ \quad (17)$$

2.12 Influence of Competing Species

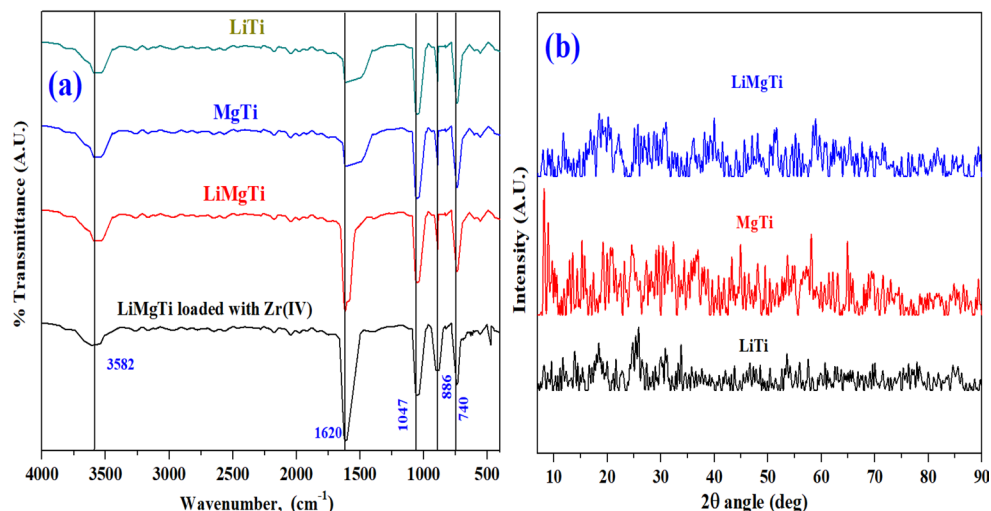
Zr(IV) ions uptake onto LiTi, MgTi, and LiMgTi sorbents was carried out by agitating Zr(IV) in the presence of various concentrations of competing ions (CaCl_2 , MgCl_2 , and NaCl), (10^{-3} , 10^{-2} , 10^{-1} , 0.5, and 1 M) at pH 2.4.

3 Results and Discussion

3.1 FT-IR Analysis

The ATR/FTIR spectrum of LiTi, MgTi, and LiMgTi sorbents was represented in Fig. 1(a). Indeed, the corresponding infrared spectrum shows an absorption band at 3582 cm^{-1} attributed to lithium hydroxide's stretching mode (νOH) [46]. The band at 1620 cm^{-1} was due to the H–OH (bending vibrations) of the adsorbed water molecules [47]; the intensity of this band increases in the case of LiMgTi than LiTi and MgTi sorbents related to increasing water content in the LiMgTi sorbent that led to high sorption behaviour of LiMgTi sorbent for Zr(IV) ions. The absorption bands at 1047 , 886 , and 740 cm^{-1} related to Ti–OH (deformation vibration) [48, 49], overlapping of Ti–O and Ti–OH [50], and Ti–O bonds, respectively [51]. The ATR/FTIR spectrum of LiMgTi sorbent loaded by Zr(IV) was shown in Fig. 1(a) and exhibits the same absorption bands noticed in the ATR/FTIR spectrum of LiMgTi sorbent without any new bands appeared for LiMgTi sorbent loaded by Zr(IV), confirming

Fig. 1 (a) ATR/FTIR spectrum and (b) XRD pattern of LiTi, MgTi, and LiMgTi sorbents



that sorption of Zr(IV) onto LiMgTi is physical adsorption on the surface of LiMgTi sorbent.

3.2 XRD Analysis

XRD analysis reflects the crystallinity and amorphous nature of LiTi, MgTi, and LiMgTi sorbents, as represented in Fig. 1(b). This Figure exhibits the amorphous nature of LiTi, MgTi, and LiMgTi sorbents without sharp peaks, and this character is the same as the XRD of the SiSb sorbent fabricated by Abass et al. [52].

3.3 SEM, EDX, and BET Analysis

The surface morphology of LiTi, MgTi, and LiMgTi sorbents was examined using SEM pictures, as shown in Fig. 2, at a magnification power of X2000. The photos show a heterogeneous distribution of the magnesium and lithium particles (white) on the titanate (grey); simply put, they resemble a swarm of tiny islands on the ocean's surface. These particles are tough and sharp, with intermolecular spacing that aids physical sorption onto LiTi, MgTi, and LiMgTi sorbents.

EDX analysis of LiTi, MgTi, and LiMgTi sorbents (Fig. 2) indicates that the percentages of Li, Mg, and Ti are nearly identical in the prepared sorbents. However, the percentage of oxygen decreases after modification, confirming the replacement of oxygen with magnesium to form LiMgTi.

The pore structure parameters, including the BET surface area and pore size of LiTi, MgTi, and LiMgTi sorbents, played a crucial role in adsorption [53]. The specific surface area for LiTi, MgTi, and LiMgTi sorbents was determined by the N₂ adsorption/desorption technique to be 101.25, 104.9, and 118.4 m² g⁻¹, respectively. At the same time, the pore size was 0.48, 0.49, and 0.51 cm³ g⁻¹ for LiTi, MgTi, and LiMgTi, respectively. These values are good results compared with the BET surface area of the microporous

zirconium silicate prepared by Hamed et al. is 158 m²/g [54] and facilitates adsorption of Zr(IV) on the surface of LiTi, MgTi, and LiMgTi sorbents as mentioned below in sorption results.

3.4 Chemical Stability

The solubility test of LiTi, MgTi, and LiMgTi sorbents toward many solvents was done using DDW, ethanol, HNO₃, and NaOH (Table 2). The results reflect that LiTi, MgTi, and LiMgTi sorbents were very stable in DDW, organic solvent (ethanol), mineral acid (HNO₃), and alkali (NaOH). Table 2 exhibits that LiTi, MgTi, and LiMgTi sorbents have relative stability to chemicals compared to other sorbents [18, 55, 56]. Also, the results show that LiMgTi sorbent is more stable than LiTi and MgTi sorbents.

3.5 Zirconium Ions Hydrolysis

The separation of Zr(IV) ions by LiTi, MgTi, and LiMgTi sorbents is mostly affected by the side reaction of Zr(IV) ions hydrolysis, mainly based on the solution pH. Thus, samples (10 mL each) containing 50 mg/L of Zr(IV) ions were prepared at pH values ranging from 0.5 to 4. After 0.5 h of mixing time, each sample was filtered, and the concentrations of Zr(IV) ions were detected spectrophotometrically to compute the precipitation % (Table 3). From the data represented in Table 3, it can be seen that Zr(IV) ions precipitated above pH 2.5. As indicated by Zr(IV) hydrolysis results, all experiments were carried out at pH 2.4 to avoid the hydrolysis of the Zr(IV) ions.

3.6 Influence of pH

The sorption efficiency (% S.E.) of Zr(IV) ions onto LiTi, MgTi, and LiMgTi sorbents from aqueous media at different

Fig. 2 SEM pictures and EDX analysis for (a) LiTi, (b) MgTi, and (c) LiMgTi sorbents

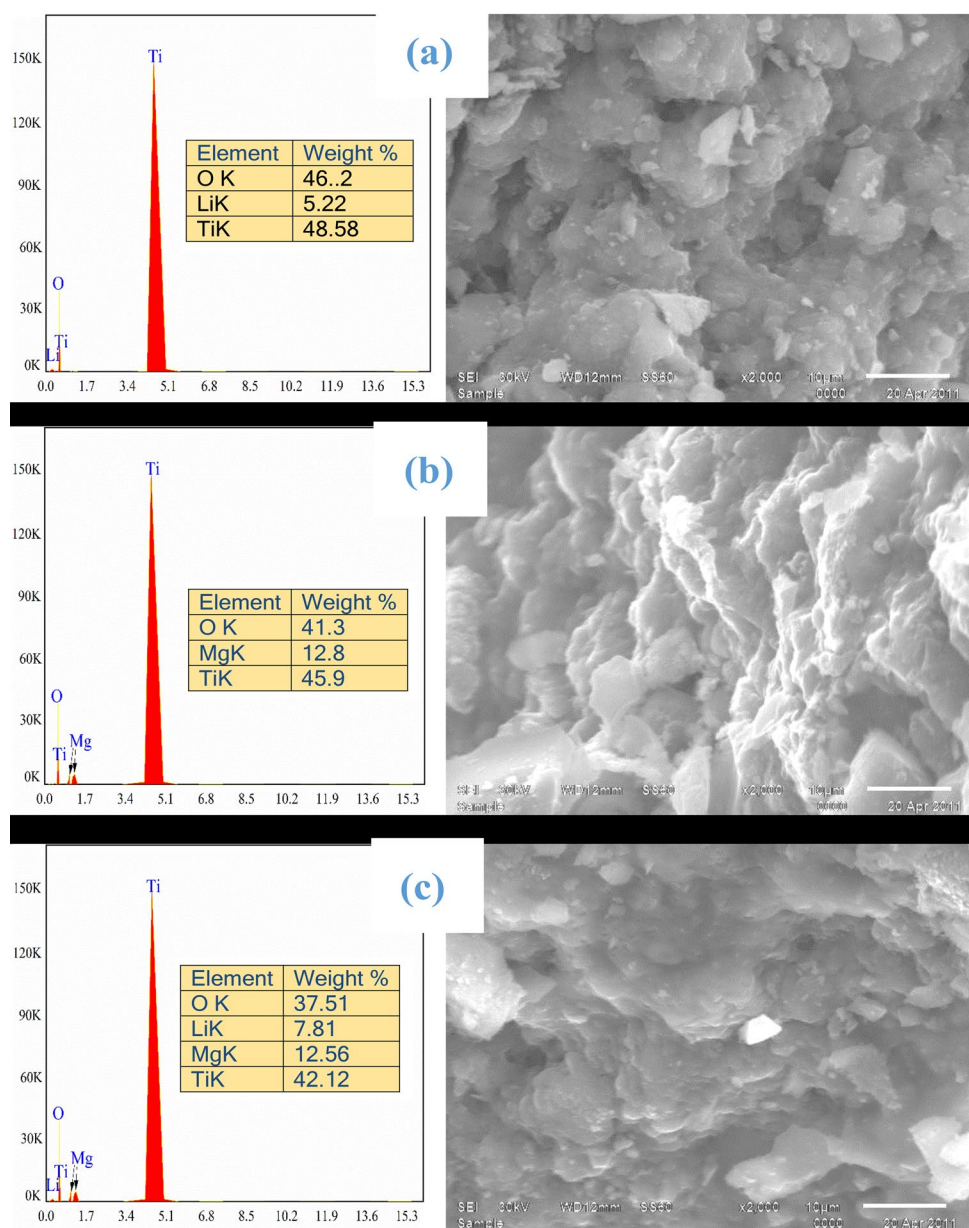


Table 2 Chemical stability of LiTi, MgTi, and LiMgTi sorbents in different solvents

Solvents	Solubility, (g/L)		
	LiTi	MgTi	LiMgTi
DDW	B.D.L.	B.D.L.	B.D.L.
Ethanol	B.D.L.	B.D.L.	B.D.L.
0.5 mol/L HNO ₃	0.125	0.121	0.118
1 mol/L HNO ₃	0.143	0.133	0.126
2 mol/L HNO ₃	0.178	0.164	0.139
0.5 mol/L NaOH	0.142	0.132	0.128
1 mol/L NaOH	0.172	0.143	0.141
2 mol/L NaOH	0.191	0.183	0.178

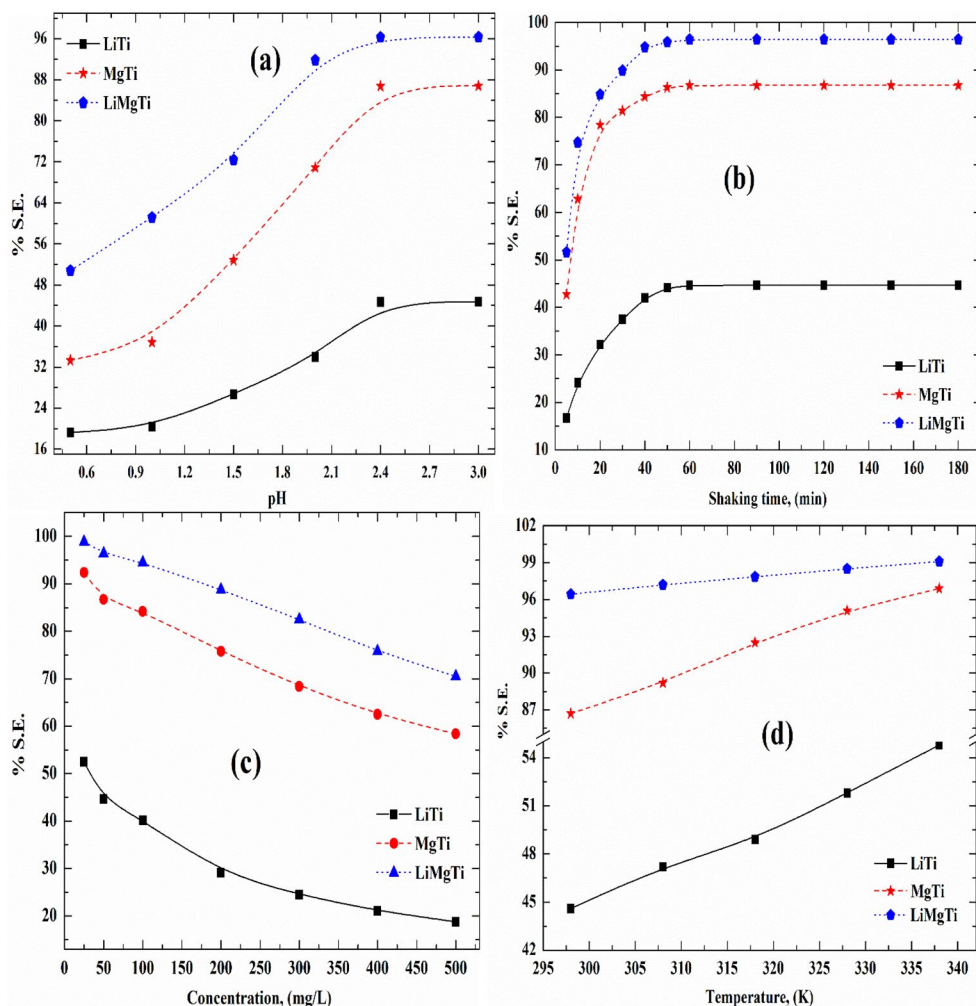
Where B.D.L. indicates below detection limit

Table 3 Zr(IV) hydrolysis (%) at different pH values

pH	Zr(IV)
0.5	Nil
1.0	Nil
1.5	Nil
2.0	Nil
2.5	8.5
3.0	22.4

pHs was done as shown in Fig. 3(a). % S.E. increase with rising pHs from (0.5–2.4) [(19.2–44.6%) for LiTi, (33.3–86.8%) for MgTi, and (50.8–96.3%) for LiMgTi]. According to the results presented in Table 3, Zr(IV) ions start to precipitate as hydroxide at pH above 2.4. Also, at low pH levels, the % S.E. of Zr(IV) is low, which is likely owing

Fig. 3 Sorption of Zr(IV) ions onto LiTi, MgTi, and LiMgTi sorbents (a) effect of pH on the % S.E., (b) effect of shaking time on the % S.E., (c) effect of initial concentration on the % S.E., and (d) effect of pH on the % S.E.



to protonation of the surface active sites and an increase in H_3O^+ ions in the aqueous solution. As pH values increased, the concentration of H_3O^+ ions reduced while the concentration of OH^- ions increased, causing sorbent surface deprotonation. These findings indicate that the surface of the LiTi, MgTi, and LiMgTi sorbents possesses a negative charge. Also, the data in Fig. 3(a) suggest that LiMgTi sorbent has higher S.E. than LiTi and MgTi at all pH values.

3.7 Influence of Shaking Time

The effect of contact time on % S.E. of Zr(IV) ions onto LiTi, MgTi, and LiMgTi sorbents was done at constant temperature (298 ± 1 K), $C_0 = 50$ mg/L, $V/m = 100$ mL/g, contacting time (5–180 min), and $\text{pH} = 2.4$, the attained results are represented in Fig. 3(b). The data show that the % S.E. of Zr(IV) ions increases with mixing time, reaching an equilibrium of ~ 1 h. The rate of Zr(IV) ions uptake onto LiTi, MgTi, and LiMgTi sorbents very rapidly improved with time from 5 to 40 min and slowly improved from 50 min to 1 h, so 1 h was used as equilibrium time for further experimental

work due to no change in S.E. above this time. Also, the data in Fig. 3(b) reveal that LiMgTi sorbent has higher S.E. than LiTi and MgTi at all times.

3.8 Effect of Concentrations and Temperature

Figure 3(c) reveals the plots between % S.E. of Zr(IV) ions onto LiTi, MgTi, and LiMgTi sorbents and C_0 at the range (25–500 mg/L), temperature (298 ± 1 K), $V/m = 100$ mL/g, mixing time (60 min), and $\text{pH} = 2.4$. The % S.E. of Zr(IV) ions onto LiTi, MgTi, and LiMgTi sorbents decreases as the initial concentration increases. These data reflect that the % S.E. is very high at a small initial concentration due to low competition. Also, the data in Fig. 3(c) reflect that LiMgTi sorbent has higher sorption efficiency than LiTi and MgTi at all concentrations. Figure 3(d) reveals the plots between % S.E. of Zr(IV) ions onto LiTi, MgTi, and LiMgTi sorbents and reaction temperatures at the range (298–338 K) at a fixed concentration ($C_0 = 50$ mg/L, $V/m = 100$ mL/g, time (60 min), and $\text{pH} = 2.4$). The % S.E. of Zr(IV) ions onto LiTi, MgTi, and LiMgTi sorbents increase as temperature

increases, proving the endothermic nature of the sorption. Also, the data in Fig. 3(d) reflect that LiMgTi sorbent has higher sorption efficiency than LiTi and MgTi at all reaction temperatures.

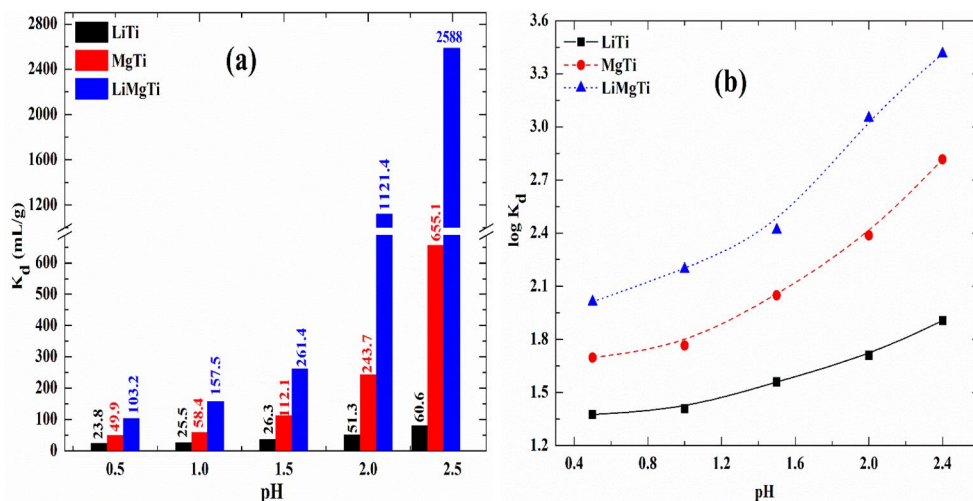
3.9 Saturation Capacity

The saturation capacity of Zr(IV) ions onto LiTi, MgTi, and LiMgTi sorbents was determined at $(298 \pm 1 \text{ K}, \text{pH } 2.4)$. The data reflect that the saturation capacity for Zr(IV) ions onto LiTi, MgTi, and LiMgTi sorbents was 12.9, 36.6, and 39.4 mg/g, respectively. These data reflect a great enhancement of saturation capacity when magnesium ions are impregnated into LiTi sorbent.

3.9.1 Distribution Coefficients (K_d) Studies

Figure 4(a) shows the variation in the values of K_d for Zr(IV) ions onto LiTi, MgTi, and LiMgTi sorbents as a function of pH. The K_d increases with increasing pH values. At small $\text{pH} \leq 1.5$, K_d of Zr(IV) ions small enhances; this is related to the presence of excess protons competing with Zr(IV) ions in the solution and preferably occupying the binding sites available in LiTi, MgTi, and LiMgTi sorbents [33, 57]. At a higher pH greater than 1.5, K_d constantly increases with rising pH due to reduced proton competition. Also, the data in Fig. 4(a) reflect that LiMgTi sorbent has higher K_d than LiTi and MgTi at all pH values. Nonlinear relations between $\log K_d$ and pH were noticed for Zr(IV) ions, as shown in Fig. 4(b). This relationship proves the exchange reaction's non-ideality. This approach could be due to the prominence of a mechanism other than ion exchange, like precipitation and surface adsorption [58].

Fig. 4 Sorption of Zr(IV) ions onto LiTi, MgTi, and LiMgTi sorbents (a) effect of pH on the distribution coefficients and (b) plots of $\log K_d$ against pH



3.10 Kinetic Study

PFO, PSO, and Elovich equations were used to examine the adsorption kinetics and the experimental data. Zr(IV) adsorption onto LiTi, MgTi, and LiMgTi sorbents occurred at 2 stages, as represented in Fig. 5. Rapid adsorption occurred throughout the first 40 min of the experiment. Adsorption was longer and slower in the second phase, possibly involving the adsorbent's interior. The first stage was quick and quantitatively dominant, whereas the second was slower and numerically inconsequential. During the first adsorption stage, many active centres were available on the surface of LiTi, MgTi, and LiMgTi sorbents. After these centres were occupied, the equilibrium condition was reached, and the second stage, including the sorbents' inner areas, began. When the correlation coefficients (R^2) of the PFO and PSO models (Table 4) were examined, it was discovered that the PFO kinetic model fit the results better than the PSO kinetic model. Furthermore, the similarity of the theoretically estimated and practical q_e values demonstrated agreement with the PFO model. These findings showed that the adsorption process followed PFO rate kinetics. The data in Table 4 declared that the Elovich equation did not fit the experimental results based on the low values of (R^2). This validated the inapplicability of this model for describing the sorption of Zr(IV) onto LiTi, MgTi, and LiMgTi sorbents.

3.11 Sorption Isotherms

The Langmuir and Freundlich isotherm models were utilised to investigate the equilibrium data and establish an appropriate design model. R^2 indicates that isotherm equations are applicable. Adsorption isotherms demonstrated the interaction mechanism at equilibrium between LiTi, MgTi, and LiMgTi sorbents and Zr(IV) ions. When the R^2 values from the Langmuir and Freundlich isotherm models are compared (Fig. 6; Table 5), the adsorption process

Fig. 5 Kinetic modeling fitting of Zr(IV) ions onto LiTi, MgTi, and LiMgTi sorbents at $[C_0 = 50 \text{ mg/L}$, $V/m = 100 \text{ mL/g}$, shaking time (5–180 min), pH 2.4, and $25 \pm 1 \text{ }^\circ\text{C}$

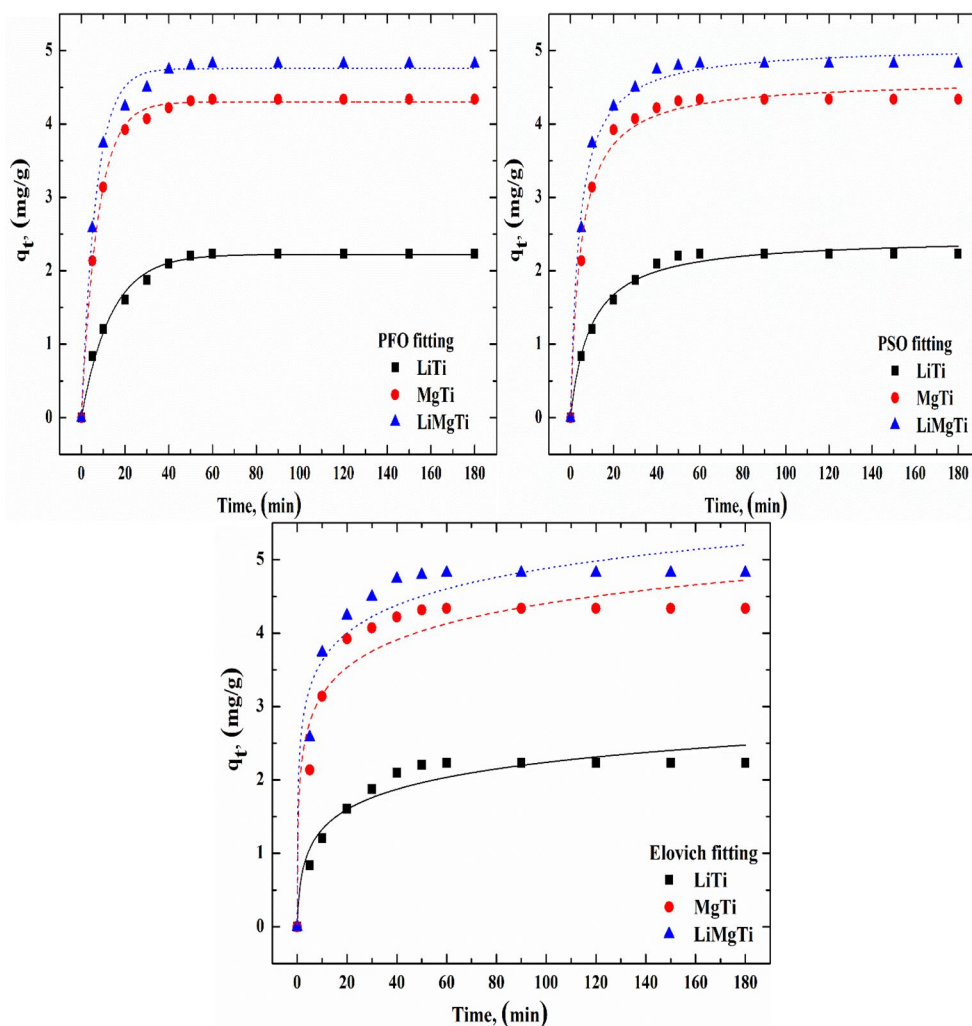


Table 4 Kinetic parameters for Zr(IV) ions onto LiTi, MgTi, and LiMgTi sorbents

Sorbents	PFO	q_e (exp.)	PSO	Elovich
LiTi	q_e (cal.)	2.22	q_e (cal.)	α 1.04
	K_1	0.073	K_2	β 2.48
	H_1	0.163	H_2	R^2 0.937
	R^2	0.990	R^2	
MgTi	q_e (cal.)	4.30	q_e (cal.)	α 18.46
	K_1	0.131	K_2	β 1.847
	H_1	0.563	H_2	R^2 0.934
	R^2	0.998	R^2	
LiMgTi	q_e (cal.)	4.755	q_e (cal.)	α 41.27
	K_1	0.148	K_2	β 1.829
	H_1	0.706	H_2	R^2 0.947
	R^2	0.993	R^2	

according to the Freundlich isotherm model gave a superior fit with the Freundlich model ($R^2 = 0.992$, 0.995 , and 0.995) for LiTi, MgTi, and LiMgTi sorbents, respectively. K_F , a measure of adsorption capacity, was 0.48, 2.1, and 4.87, and $1/n$, which were 0.499, 0.496, and 0.40. The $1/n$ numbers indicated that the conditions were favourable for

adsorption. Also, the adsorption process conformed to the Langmuir isotherm model ($R^2 = 0.989$, 0.986 , and 0.973) for LiTi, MgTi, and LiMgTi sorbents, respectively. R_L values were found to be (0.209, 0.114, and 0.046) reflecting the favourable sorption isotherms of Zr(IV) [59]. The maximum adsorption capacity was 12.0, 36.6, and 38.7 mg/g for

Fig. 6 Isothermal modeling fitting of Zr(IV) ions onto LiTi, MgTi, and LiMgTi sorbents [Eq. time = 60 min, V/m = 100 mL/g, pH = 2.4]

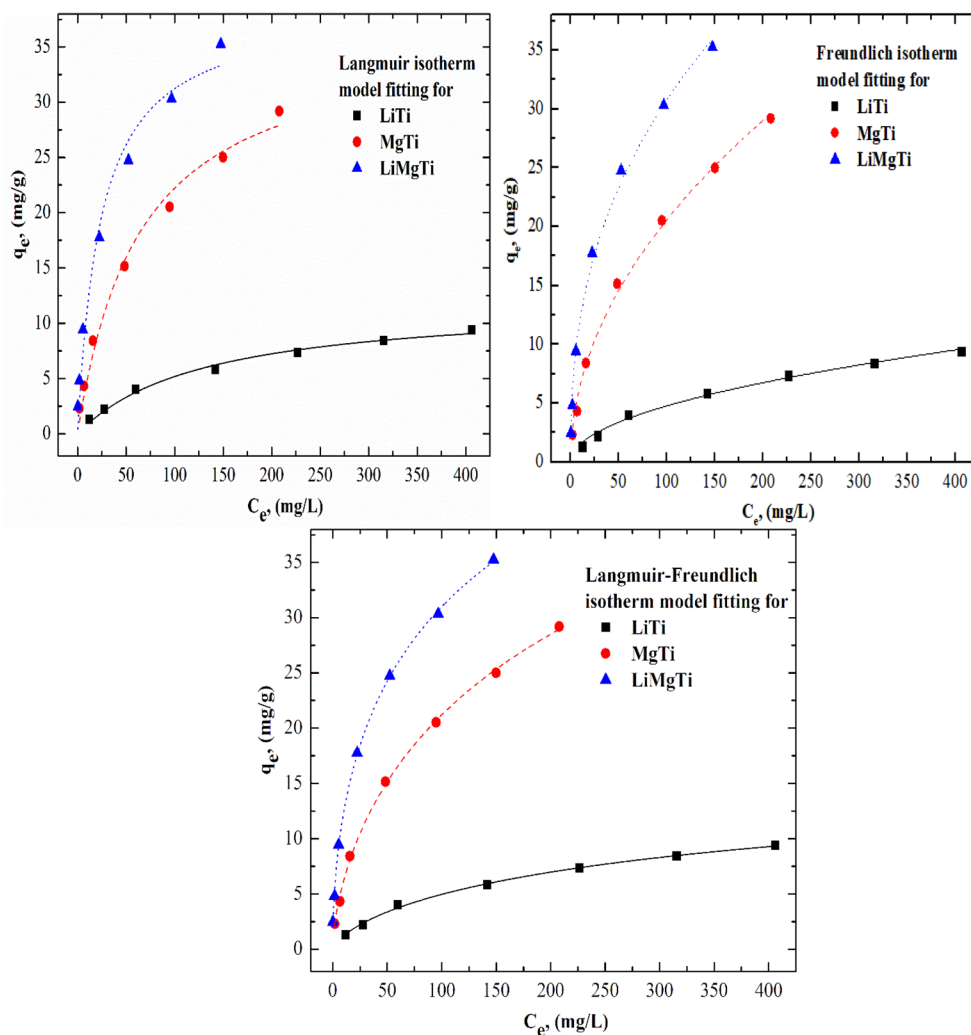


Table 5 Isotherm parameters for sorption of Zr(IV) ions onto LiTi, MgTi, and LiMgTi sorbents

Sorbents	Langmuir				Freundlich			Langmuir–Freundlich			
	K_L	q_m	R_L	R^2	$1/n$	K_F	R^2	q_m	K_{LF}	m	R^2
LiTi	0.0076	12.0	0.209	0.989	0.499	0.48	0.992	19.314	0.002	0.710	0.997
MgTi	0.0155	36.6	0.114	0.986	0.496	2.10	0.995	73.244	0.002	0.645	0.998
LiMgTi	0.0416	38.7	0.046	0.973	0.40	4.87	0.995	80.096	0.004	0.541	0.999

LiTi, MgTi, and LiMgTi sorbents. The different parameters of the Langmuir–Freundlich isotherm model for sorption of Zr(IV) onto LiTi, MgTi, and LiMgTi sorbents were evaluated by plotting q_e vs. C_e , and data are presented in Fig. 6. The values of these parameters along with correlation coefficients were determined from the non-linear plots and listed in Table 5. The values of m deviate from unity; therefore, the Langmuir–Freundlich isotherm model was converted to the Freundlich isotherm model. The graphical presentations show a good fitting between the Langmuir–Freundlich isotherm model and experimental data over the Zr(IV) studied concentrations. This is due to the extremely high values of correlation coefficients ($R^2 = 0.997–0.999$). Meanwhile, the q_m values of LiTi, MgTi, and LiMgTi sorbents towards

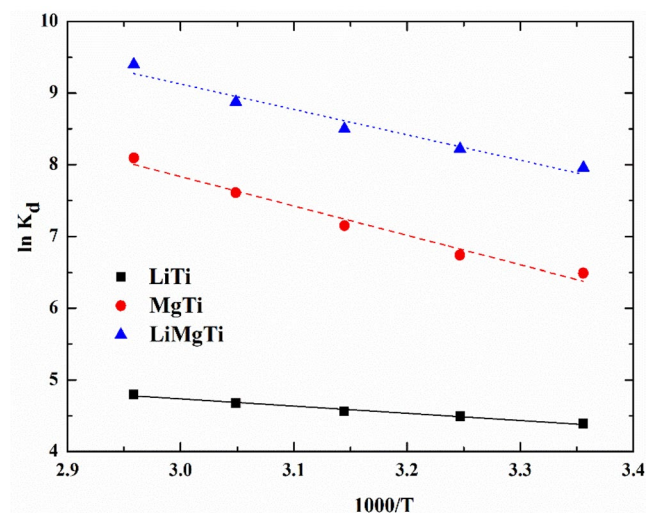
Zr(IV) obtained using the Langmuir–Freundlich isotherm model deviated from their experimental values. Based on these results, the sorption isotherm of Zr(IV) onto synthesised sorbents could be explained by the Freundlich isotherm model.

3.12 Comparison of Maximum Sorption Capacity with Different Sorbents

The maximum sorption capacity of LiTi, MgTi, and LiMgTi sorbents for Zr(IV) sorption was compared with other sorbents reported in the literature. As represented in Table 6, the maximum sorption capacity of LiTi, MgTi, and LiMgTi sorbents is higher than the previously reported values, which

Table 6 Comparison of the maximum sorption capacity of Zr(IV) sorbed onto various sorbents

Sorbents	Maximum sorption capacity, mg/g	Ref. no.
LiTi	12.0	Current work
MgTi	36.6	Current work
LiMgTi	38.7	Current work
Natural clinoptilolite	8.312	[60]
TANB	15.432	[19]
FeSnSi	41.3	[61]
Bentonite	63.35	[62]
Rice bran	50.0	[63]

**Fig. 7** Van't Hoff plot for the adsorption of Zr(IV) ions onto LiTi, MgTi, and LiMgTi sorbents

suggests that these are promising sorbents to remove Zr(IV) from aqueous solutions [19, 60–62].

3.13 Thermodynamic Studies

Temperatures of 298, 308, 318, 328, and 338 K were utilised to analyse the thermodynamic behaviour of the adsorption process, as shown in Fig. 7. For LiTi, MgTi, and LiMgTi sorbents, the change in ΔH° during the adsorption process was 8.4, 34.1, and 29.5 kJ mol⁻¹, respectively. The temperature rise favourably influences Zr(IV) elimination in the endothermic adsorption process; the amount adsorbed increases with rising temperature. The entropy change, ΔS° , for LiTi, MgTi, and LiMgTi sorbents was 64.5, 167.3, and 164.3 Jmol⁻¹ K⁻¹. This finding revealed that the adsorption process was random. A positive entropy could be regarded as an increase in the adsorption system's randomness due to the adsorbent's high affinity [64]. Gibbs free energy, ΔG° was -10.8, -11.5, -12.1, -12.8, and -13.4 kJ mol⁻¹ for LiTi, -15.8, -17.5, -19.1, -20.8, and -22.5 kJ mol⁻¹ for MgTi, and -19.5, -21.1, -22.8, -24.4, and -26.1 kJ mol⁻¹ for LiMgTi. The increased mobility of Zr(IV) ions sorbed onto the LiTi, MgTi, and LiMgTi sorbents surface,

Table 7 Effect of NaCl, MgCl₂, and CaCl₂ on sorption of Zr(IV) ions onto LiTi, MgTi, and LiMgTi sorbents at 25 ± 1 °C

Sorbents	Concentration of interfering ions, [M]	% S.E.			
		Blank	CaCl ₂	MgCl ₂	NaCl
LiTi	1	44.5	4.65	5.35	10.5
	0.5		9.58	11.52	22.5
	0.1		14.58	14.6	30.5
	0.01		31.5	32.5	38.5
	0.001		42.1	42.55	43.2
MgTi	1	86.7	10.6	12.5	14.8
	0.5		25.6	28.5	35.4
	0.1		45.6	51.5	58.9
	0.01		63.2	68.6	71.5
	0.001		78.5	81.2	85.1
LiMgTi	1	96.6	15.8	18.6	25.9
	0.5		34.8	40.5	51.5
	0.1		46.9	48.5	66.4
	0.01		75.8	80.6	82.9
	0.001		88.2	92.8	94.5

as well as increased electrostatic interaction between Zr(IV) ions and different functional groups on the LiTi, MgTi, and LiMgTi sorbents surface, resulted in improved ΔG° availability at higher temperatures.

3.14 Influence of Interfering Ions

The effect of CaCl₂, MgCl₂, and NaCl at different concentrations (10⁻³, 10⁻², 10⁻¹, 0.5, and 1 M) on the % S.E. of Zr(IV) at pH 2.4 was investigated utilising LiTi, MgTi, and LiMgTi sorbents. Table 7 displays the changes in the % S.E. in the presence of CaCl₂, MgCl₂, and NaCl, and the data indicated that the % S.E. of Zr(IV) is greatly reduced by increasing the concentration of MgCl₂ and CaCl₂. These results may be explained based on the competition of Ca(II) and Mg(II) ions for the LiTi, MgTi, and LiMgTi surfaces. Besides, it was found that LiTi, MgTi, and LiMgTi show a high affinity for Zr(IV) in the presence of Na(I) over a wide range of concentrations; this may be due to the high preference for tetravalent cations on three sorbents, and so Zr(IV) compete for suitable space in the structure also, that the % S.E. of Zr(IV) on LiTi, MgTi, and LiMgTi sorbents are affected in the order NaCl > MgCl₂ > CaCl₂.

4 Conclusion

In this article, the LiTi, MgTi, and LiMgTi sorbents were fabricated using the precipitation technique and used for the sorption of Zr(IV) ions from aqueous solutions. The sorption data of Zr(IV) ions confirm that LiTi, MgTi, and LiMgTi sorbents have a contact time of 60 min, pH dependence, applicable to the Freundlich isotherm model, and more fitted to the PFO kinetic model. Saturation capacity experiments illustrate that the maximum Zr(IV) ions sorbed onto LiTi, MgTi, and LiMgTi sorbents were 12.9, 36.6, and 39.4 mg/g, respectively. Thermodynamic parameters data reveal that the sorption process was endothermic and spontaneous. Finally, the sorption efficiency of Zr(IV) was affected by the presence of some competing species, such as CaCl₂, MgCl₂, and NaCl. The previously mentioned data demonstrates that the LiMgTi sorbent is a material with great potential for the sorption of Zr(IV) from aqueous solutions.

Acknowledgements I want to thank all the Nuclear Fuel Technology department members at the Egyptian Atomic Energy Authority for supporting this work.

Author Contributions M.R. Abass: Conceptualization, Visualization, experimental work, writing-reviewing, and editing. A.B. Ibrahim: Experimental work, Data curation, writing - original draft review and editing. M.M. Abou-Mesalam: Editing, and reviewing.

Funding Not applicable.

Open access funding provided by The Science, Technology & Innovation Funding Authority (STDF) in cooperation with The Egyptian Knowledge Bank (EKB).

Data Availability Yes.

Declarations

Ethical Approval Yes.

Consent to Participate Yes.

Consent to Publish Yes.

Competing Interests The authors whose names are listed immediately below certify that they have NO affiliations with or involvement in any organisation or entity with any financial interest (such as honoraria, educational grants, participation in speakers' bureaus, membership, employment, consultancies, stock ownership, or other equity interest; and expert testimony or patent-licensing arrangements), or non-financial interest (such as personal or professional relationships, affiliations, knowledge or beliefs) in the subject matter or materials discussed in this manuscript.

Open Access This article is licensed under a Creative Commons Attribution 4.0 International License, which permits use, sharing, adaptation, distribution and reproduction in any medium or format, as long as you give appropriate credit to the original author(s) and the source, provide a link to the Creative Commons licence, and indicate if changes were made. The images or other third party material in this

article are included in the article's Creative Commons licence, unless indicated otherwise in a credit line to the material. If material is not included in the article's Creative Commons licence and your intended use is not permitted by statutory regulation or exceeds the permitted use, you will need to obtain permission directly from the copyright holder. To view a copy of this licence, visit <http://creativecommons.org/licenses/by/4.0/>.

References

- M.R. Abass, M.M.E. Breky, R.M. Maree, *Appl. Radiat. Isot.* **189**, 110417 (2022)
- M.A. Hamoud, K.F. Allan, W.A. Sanad, S.H. El-Hamouly, R.R. Ayoub, *J. Radioanal. Nucl. Chem.* **302**, 169 (2014)
- M.S. Mansy, R.S. Hassan, Y.T. Selim, S.H. Kenawy, *Appl. Radiat. Isot.* **130**, 198 (2017)
- A.A. El-Sadek, M.R. El-Naggar, M.S. Mansy, *Appl. Radiat. Isot.* **172**, 109690 (2021)
- S.S. Mahrous, M.R. Abass, M.S. Mansy, *Appl. Radiat. Isot.* **190**, 110445 (2022)
- H. Moloukhia, W.S. Hegazy, E.A. Abdel-Galil, S.S. Mahrous, *Chem. Ecol.* **32**, 324 (2016)
- J.M. Ahn, S. Kim, Y.-S. Kim, *Environ. Geochem. Health* **1** (2019)
- A.E. Osmanlioglu, *Nucl. Eng. Technol.* **50**, 886 (2018)
- S. Hurtado-Bermúdez, M. Villa-Alfageme, J.L. Mas, M.D. Alba, *Appl. Radiat. Isot.* **137**, 177 (2018)
- P.B. Vilela, A. Dalalibera, E.C. Duminelli, V.A. Becegato, A.T. Paulino, *Environ. Sci. Pollut. Res.* **26**, 28490 (2019)
- N.K. Gupta, A. Gupta, P. Ramteke, H. Sahoo, A. Sengupta, *J. Mol. Liq.* **274**, 148 (2019)
- M.H.A. Aziz, M.H.D. Othman, N.A. Hashim, M.R. Adam, A. Mustafa, *Appl. Clay Sci.* **177**, 51 (2019)
- M.R. Abass, E.H. El-Masry, W.M. El-Kenany, *J. Inorg. Organomet. Polym. Mater.* **32**, 536 (2022)
- M.R. Abass, R.A. Abou-Lilah, A.E. Kasem, *Russ J. Inorg. Chem.* **1** (2024)
- C. Miyake, M. Hirose, T. Yoshimura, M. Ikeda, S. Imoto, M. Sano, *J. Nucl. Sci. Technol.* **27**, 157 (1990)
- Y. Hu, X. Bai, Y. Chen, W. Wang, Q. Chen, Z. Cao, T. Yan, *Nanomaterials.* **14**, 13 (2023)
- S. Mishra, A.K. Soda, M. Sridhar, C. Mallika, N.K. Pandey, U.K. Mudali, *Solvent Extr. Ion Exch.* **36**, 54 (2018)
- A.B. Ibrahim, M.R. Abass, E.H. EL-Masry, M.M. Abou-Mesalam, *Appl. Radiat. Isot.* **178**, 109956 (2021)
- R. Donat, *Russ J. Phys. Chem. A* **96**, 2974 (2022)
- D.M. Demerdash, *Egypt. J. Chem.* **66**, 435 (2023)
- X. Hu, Q. Zhang, Y. Yu, Y. Hu, Y. Wang, *Chem. Phys. Lett.* **752**, 137585 (2020)
- O.O. Shichalin, S.B. Yarusova, N.P. Ivanov, E.K. Papynov, A.A. Belov, S.A. Azon, I.Y. Buravlev, A.V. Myagchilov, A.N. Fedorets, V.L. Rastorguev, *J. Water Process. Eng.* **59**, 105042 (2024)
- E.H. Borai, R. Harjula, A. Paaanen, *J. Hazard. Mater.* **172**, 416 (2009)
- G. Liu, H. Mei, X. Tan, H. Zhang, H. Liu, M. Fang, X. Wang, *J. Mol. Liq.* **262**, 476 (2018)
- S. İnan, Y. Altaş, *Chem. Eng. J.* **168**, 1263 (2011)
- S. Chitra, S. Viswanathan, S. Rao, P. Sinha, *J. Radioanal. Nucl. Chem.* **287**, 955 (2011)
- V. Avramenko, S. Bratskaya, V. Zhelezov, I. Sheveleva, O. Voitenko, V. Sergienko, *J. Hazard. Mater.* **186**, 1343 (2011)
- D. Banerjee, U. Sandhya, S. Pahan, A. Joseph, A. Ananthanarayanan, J.G. Shah, *J. Radioanal. Nucl. Chem.* **311**, 893 (2017)
- Y. Xie, C. Chen, X. Ren, X. Wang, H. Wang, X. Wang, *Prog. Mater. Sci.* **103**, 180 (2019)

30. J. Li, X. Wang, G. Zhao, C. Chen, Z. Chai, A. Alsaedi, T. Hayat, X. Wang, *Chem. Soc. Rev.* **47**, 2322 (2018)
31. A.E. Kasem, E.A. Abdel-Galil, N. Belacy, N.A. Badawy, *Radiochim Acta.* **109**, 85 (2021)
32. M.R. Abass, R.M. Maree, N.M. Sami, *Int. J. Environ. Anal. Chem.* **104**, 103 (2024)
33. S.S. Metwally, H.S. Hassan, N.M. Samy, *J. Mol. Liq.* **287**, 110941 (2019)
34. M.R. Abass, A.B. Ibrahim, E.H. El-Masry, M.M. Abou-Mesalam, *J. Radioanal Nucl. Chem.* **329**, 849 (2021)
35. M.M. Hamed, A.M. Shahr El-Din, E.A. Abdel-Galil, *J. Radioanal Nucl. Chem.* **322**, 663 (2019)
36. W.M. El-Kenany, M.R. Abass, E.A. Abdel-Galil, *Int. J. Environ. Anal. Chem.* **1** (2022)
37. S. Lagergren, K. Sven, *Vetenskapsakademiens Handl.* **24**, 1 (1898)
38. Y.S. Ho, G. McKay, *Water Res.* **34**, 735 (2000)
39. M. Manjuladevi, R. Anitha, S. Manonmani, *Appl. Water Sci.* **8**, 1 (2018)
40. I. Langmuir, *J. Am. Chem. Soc.* **40**, 1361 (1918)
41. H. Freundlich, *Z. Für Phys. Chemie.* **57**, 385 (1907)
42. G.P. Jeppu, T.P. Clement, *J. Contam. Hydrol.* **129**, 46 (2012)
43. E.A. Abdel-Galil, A.B. Ibrahim, M.M. Abou-Mesalam, *Int. J. Ind. Chem.* **7**, 231 (2016)
44. G.A. Dakrouy, E.A.A. El-Shazly, H.S. Hassan, *J. Radioanal Nucl. Chem.* **330**, 159 (2021)
45. Z.M. Şenol, S. Şimşek, *J. Polym. Environ.* **30**, 3677 (2022)
46. G. Weber, E. Sciora, J. Guichard, F. Bouyer, I. Bezverkhyy, J. Marcos Salazar, C. Dirand, F. Bernard, H. Lecoq, R. Besnard, *J. Therm. Anal. Calorim.* **132**, 1055 (2018)
47. M.R. Abass, W.M. El-Kenany, E.H. El-Masry, *Environ. Sci. Pollut Res.* **29**, 72929 (2022)
48. M.M. Abou-Mesalam, M.R. Abass, E.S. Zakaria, A.M. Hassan, *Silicon.* **14**, 7961 (2022)
49. Y.S. Al-Degs, M.I. El-Barghouthi, A.A. Issa, M.A. Khraisheh, G.M. Walker, *Water Res.* **40**, 2645 (2006)
50. M.M. Abou-Mesalam, M.R. Abass, M.A. Abdel-Wahab, E.S. Zakaria, A.M. Hassan, H.F. Khalil, *Desalin. Water Treat.* **57**, 25757 (2016)
51. M.M. Abou-Mesalam, I.M. El-Naggar, *Colloids Surf. Physicochem Eng. Asp* **215**, (2003)
52. M.R. Abass, M.A. Eid, A.B. Ibrahim, *Int. J. Environ. Anal. Chem.* **1** (2022)
53. R.S. Hassan, M.R. Abass, M.A. Eid, E.A. Abdel-Galil, *Appl. Radiat. Isot.* **178**, 109985 (2021)
54. M.M. Hamed, M. Holiel, Y.F. El-Aryan, *J. Mol. Liq.* **242**, 722 (2017)
55. E.A. Abdel-Galil, M.A. Eid, R.S. Hassan, *Part. Sci. Technol.* **38**, 113 (2020)
56. E.A. Abdel-Galil, A.B. Ibrahim, W.M. El-Kenany, *Desalin. Water Treat.* **226**, 303 (2021)
57. H. Moloukhia, *J. Radiat. Res. Appl. Sci.* **3**, 343 (2010)
58. M.M. Abou-Mesalam, M.R. Abass, M.A. Abdel-Wahab, E.S. Zakaria, A.M. Hassan, *Desalin. Water Treat.* **109**, 176 (2018)
59. M.M. Hamed, M. Holiel, Z.H. Ismail, *Radiochim Acta.* **104**, 399 (2016)
60. H. Faghihian, M. Kabiri-Tadi, *J. Hazard. Mater.* **178**, 66 (2010)
61. S.S. Mahrous, R.A. Abou-Lilah, M.R. Abass, *Adsorption* **1** (2024)
62. Z.A. Mekawy, E.A.A. El, Shazly, M.R. Mahmoud, *J. Radioanal Nucl. Chem.* **331**, 3935 (2022)
63. E. Zolfonoun, A.B. Monji, M. Taghizadeh, S.J. Ahmadi, *Min. Eng.* **23**, 755 (2010)
64. Z.M. Şenol, S. Kaya, S. Şimşek, K.P. Katin, A. Özer, R. Marzouki, *Int. J. Biol. Macromol.* **209**, 1234 (2022)

Publisher's Note Springer Nature remains neutral with regard to jurisdictional claims in published maps and institutional affiliations.